Supporting Information

Deep removal of trace C_2H_2 and CO_2 from C_2H_4 by a customized potassium exchange mordenite

Hongwei Chen,[†a] Binyu Wang,[†b] Bin Zhang,[c] Jiuhong Chen,[a] Jiabao Gui,[a] Xiufeng Shi,[c] Wenfu Yan,[b] Jinping Li,[a] and Libo Li*[a]

[a] College of Chemical Engineering and Technology, Shanxi Key Laboratory of Gas Energy Efficient and Clean Utilization, Taiyuan University of Technology, Taiyuan 030024, China.

[b] State Key Laboratory of Inorganic Synthesis and Preparative Chemistry, College of Chemistry, Jilin University, 2699 Qianjin Street, Changchun 130012, China.

[c] College of Chemistry, Taiyuan University of Technology, Taiyuan 030024, China.

*Corresponding Author.[†]These authors contributed equally.

E-mail: lilibo@tyut.edu.cn (Libo Li)

This Supporting Information Includes:

Details for experiments, characterizations and calculations

Tables S1-S6

Figures S1-S24

Materials

All chemical reagents used were of analytical grade and without further purification.

Table S1. Reagents information.

Name	Chemical formula	Manufacturer	Purity	Mass
Ammonium chloride	NH_4Cl	Innochem Co., Ltd.	AR	500 g
Potassium chloride	KCl	Innochem Co., Ltd.	AR	500 g
Cesium chloride	CsCl	Innochem Co., Ltd.	AR	500 g
Magnesium chloride	$MgCl_2$	Innochem Co., Ltd.	AR	500 g
Calcium chloride	$CaCl_2$	Innochem Co., Ltd.	AR	500 g
Strontium chloride	$SrCl_2$	Innochem Co., Ltd.	AR	500 g
Barium Chloride	$BaCl_2$	Innochem Co., Ltd.	AR	500 g
Silica sol	SiO_2	Luoyang JALON Micro-nano New Materials Co., Ltd	30wt%	30 kg
Sodium hydroxide	NaOH	China National Pharmaceutical Group Corporation	AR	500 g
Potassium hydroxide	KOH	Shanghai Aladdin Biochemical Technology Co., Ltd.	AR	500 g
Sodium aluminate	$NaAlO_2$	China National Pharmaceutical Group Corporation	AR	500 g
Potassium aluminate	$KAlO_2$	Guangdong Wengjiang Chemical Reagent Co., Ltd.	30wt%	500 mL
Aluminium hydroxide	$Al(OH)_3$	Innochem Co., Ltd.	AR	250 g
Deionized water	H_2O	China National Pharmaceutical Group Corporation	-	25 kg
COM-MOR	MOR	Zhuoran Environmental Protection (Dalian) Co.,Ltd	>99%	100 g

Large-scale synthesis of N-MOR

A 10 L reactor was used to synthesize a large-scale N-MOR. First, 101.5 g NaOH and 101.5 g $NaAlO_2$ were mixed with 4706 g deionized water in a plastic beaker with vigorous stirring. The resulting mixture was further stirred at 298 K for 30 minutes. Next, in another plastic beaker, 2837 g of 30 wt% silica sol were mixed with vigorous stirring at room temperature for 4 hours to achieve a homogeneous slurry. Finally, the slurry was transferred to the autoclave and statically crystallized at 453 K for 3 days.

Table S2. The information of the prepared samples.

Name	Salt	Con. (mol/L)	Solid/Liquid	Temp (K)	Time (h)
Li-MOR-1	LiCl	1	1 g/50 mL	298	4
K-MOR-1	KCl	1	1 g/50 mL	298	4
Cs-MOR-1	CsCl	1	1 g/50 mL	298	4
Mg-MOR-1	$MgCl_2$	1	1 g/50 mL	298	4
Ca-MOR-1	$BaCl_2$	1	1 g/50 mL	298	4
Sr-MOR-1	$SrCl_2$	1	1 g/50 mL	298	4
Ba-MOR-Ex-1	$BaCl_2$	1	1 g/50 mL	298	4
NH_4-MOR-1	NH_4Cl	1	1 g/50 mL	298	4
K-MOR-0.01	KCl	0.01	1 g/50 mL	298	4
K-MOR-0.03	KCl	0.03	1 g/50 mL	298	4
K-MOR-0.05	KCl	0.05	1 g/50 mL	298	4
K-MOR-0.07	KCl	0.07	1 g/50 mL	298	4
K-MOR-0.1	KCl	0.1	1 g/50 mL	298	4
K-MOR-0.25	KCl	0.25	1 g/50 mL	298	4
K-MOR-0.5	KCl	0.5	1 g/50 mL	298	4
K-MOR-0.75	KCl	0.75	1 g/50 mL	298	4
K-MOR-1	KCl	1	1 g/50 mL	298	4
K-MOR-1.25	KCl	1.25	1 g/50 mL	298	4
K-MOR-1.5	KCl	1.5	1 g/50 mL	298	4
K-MOR-1.75	KCl	1.75	1 g/50 mL	298	4
K-MOR-2	KCl	2	1 g/50 mL	298	4
2*-K-MOR-1	KCl	1	1 g/50 mL	298	4
3*-K-MOR-1	KCl	1	1 g/50 mL	298	4
4*-K-MOR-1	KCl	1	1 g/50 mL	298	4

[*] Times of ions exchanged under the same conditions.

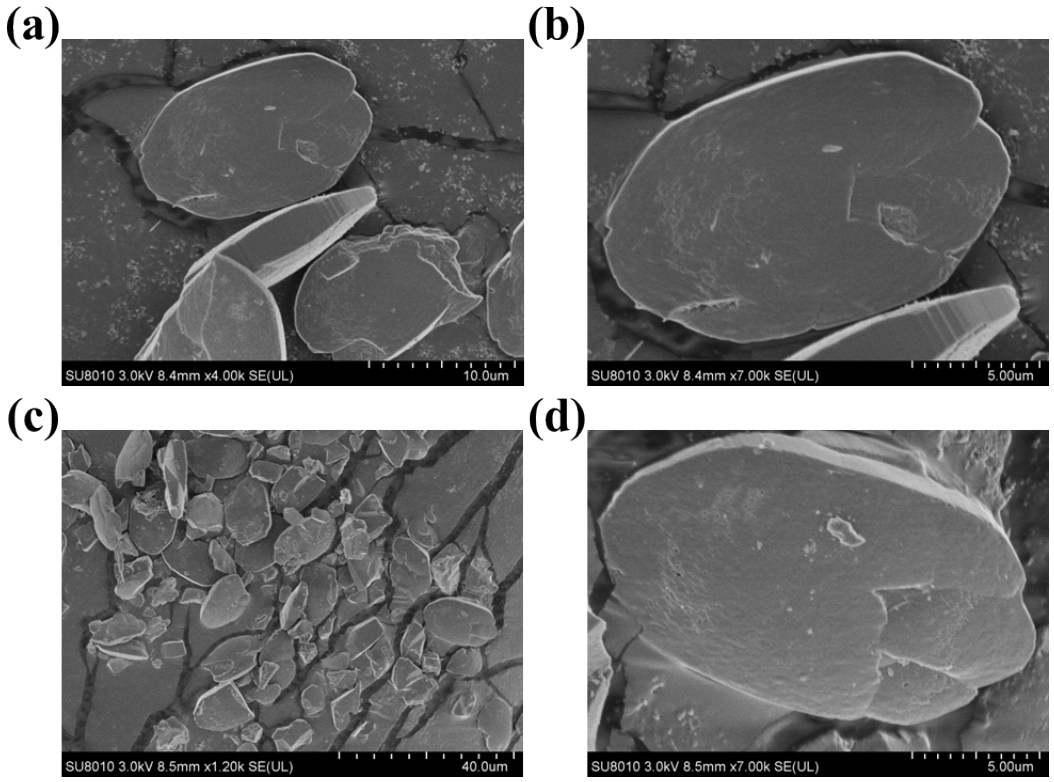

Fig. S1. The SEM images of (a-b) N-MOR and (c-d) K-MOR-1.

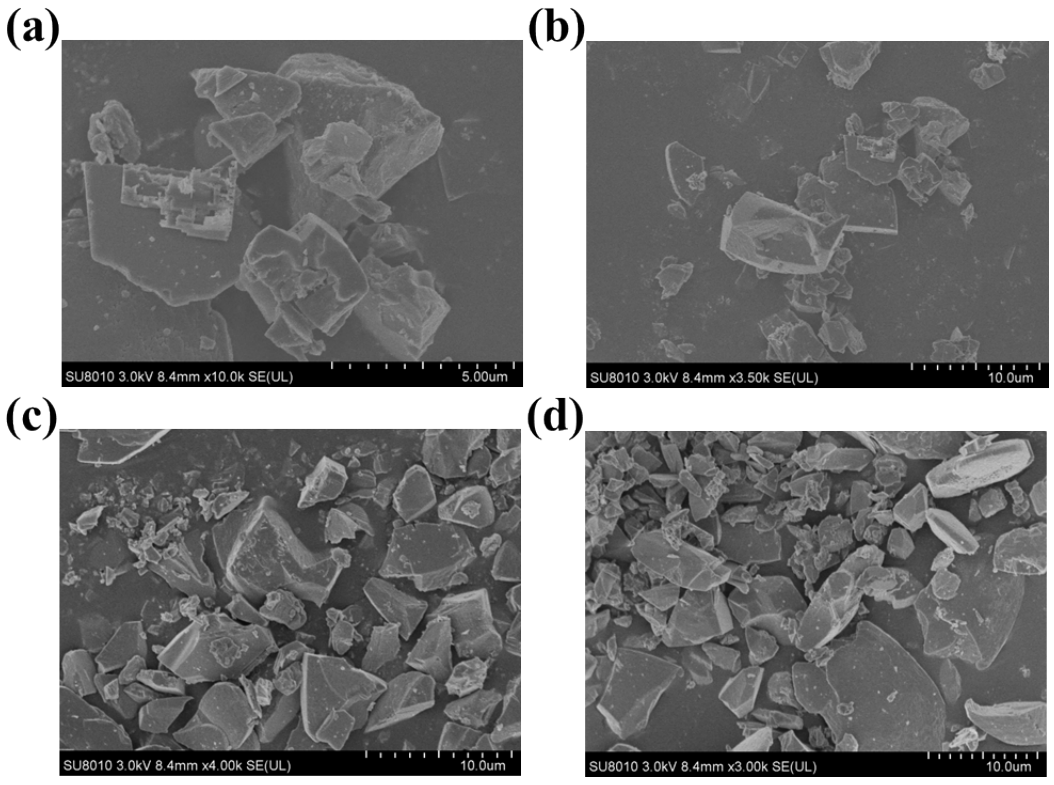

Fig. S2. The SEM images of (a-b) Li-MOR-1 and (c-d) Cs-MOR-1.

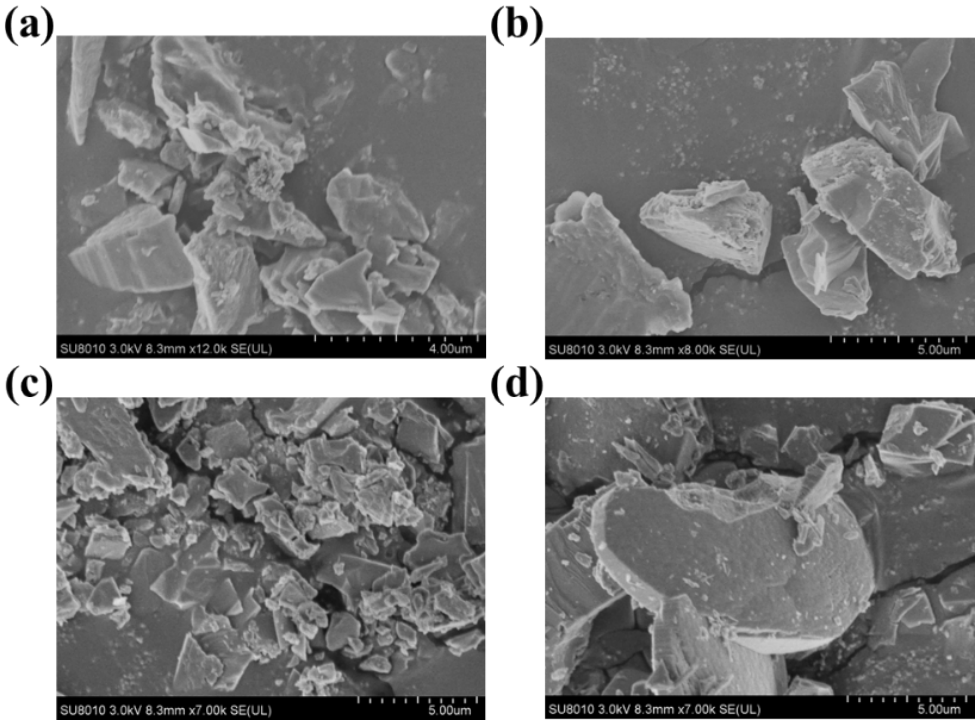

Fig. S3. The SEM images of (a-b) Sr-MOR-1 and (c-d) Ba-MOR-1.

Thermogravimetric analysis

Thermal stability was evaluated by conducting thermogravimetric (TG) analysis on an STA449F5 instrument with a constant flow of nitrogen, while the sample was heated at a rate of 10 K/min.

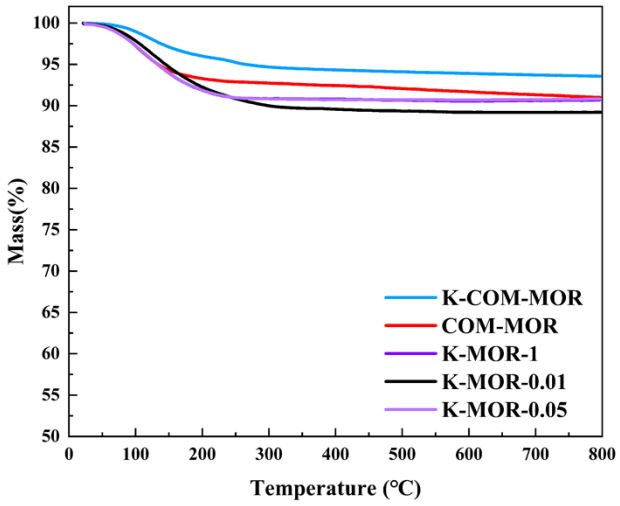

Fig. S4. TG curves.

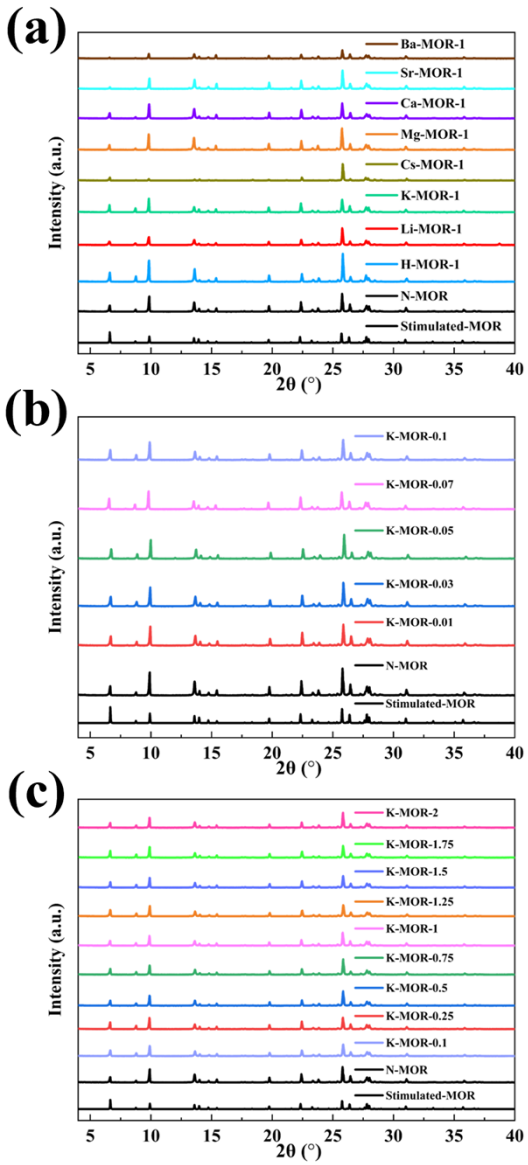

Fig. S5. (a) Simulated XRD pattern and experimental XRD patterns of N-XRD and M-MOR, (b-c) Simulated XRD pattern and experimental XRD patterns of K-MOR-X and N-MOR.

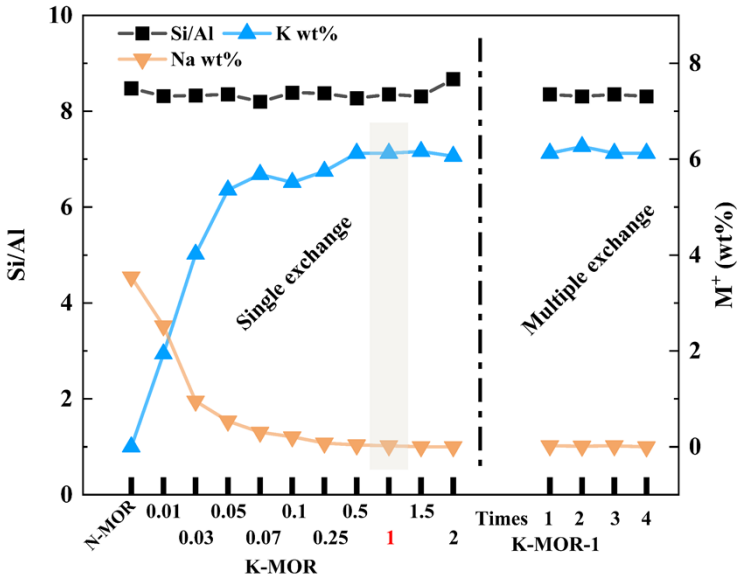

Fig. S6. Element analysis by ICP.

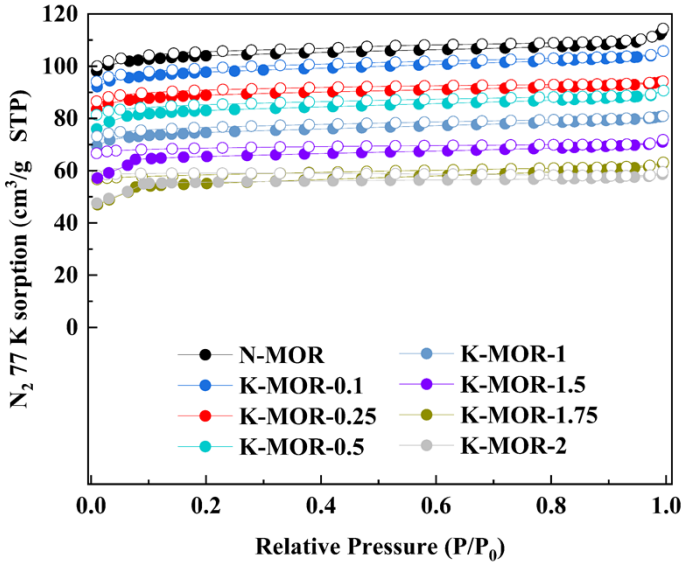

Fig. S7. N_2 sorption isotherms (77 K) of K-MOR-X (X = 0.1, 0.25, 0.5, 1, 1.5, 1.75, and 2) and N-MOR.

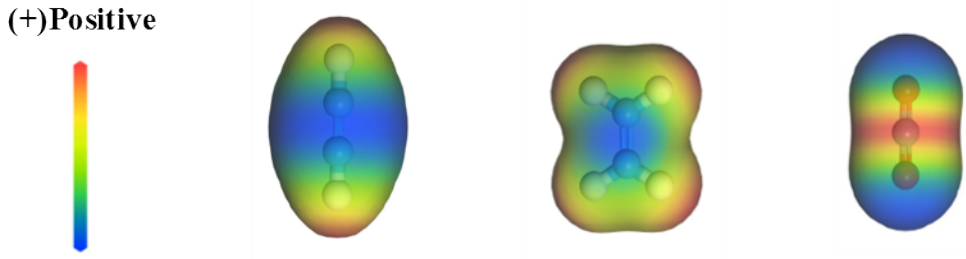

	C_2H_2	C_2H_4	CO_2
Size (Å^3)	3.32 × 3.34 × 5.70	3.28 × 4.18 × 4.84	3.18 × 3.33 × 5.37
Kinetic diameter (Å)	3.3	4.2	3.3
Boiling point (K)	189.3	194.7	169.4

Fig. S8. Information of guest molecules and electrostatic potential distribution.

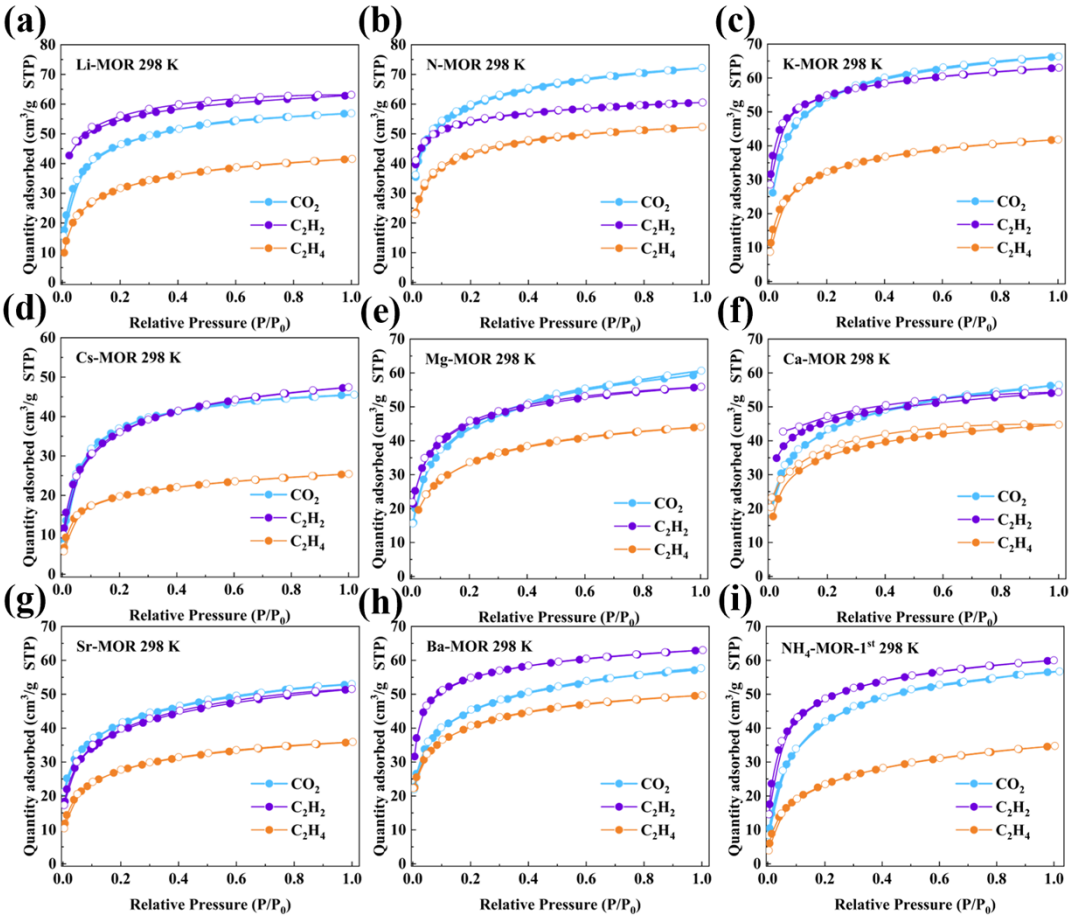

Fig. S9. Single component sorption isotherms of CO_2, C_2H_2, and C_2H_4 on M-MOR at 298 K.

Sample stability characterization

The samples were subjected to exposure to air and immersion in water. The structural integrity of the samples was evaluated using XRD, while their adsorption properties were characterized using ASAP 2020. Different pH values were achieved by preparing solutions with different concentrations of NaOH and HNO_3 aqueous solutions. Subsequently, 1 g of sample was added to 50 mL of the solution and stirred for 48 hours. The structural integrity of the solution was characterized using XRD, while the adsorption properties were evaluated using ASAP 2020. Before adsorption, the samples (1.0 g) were ion-exchanged using the KCl aqueous solution (1 mol/L, 50 mL) at 353 K for 8 hours under vigorous stirring to compensate for changes in equilibrium ions arising from pH variability.

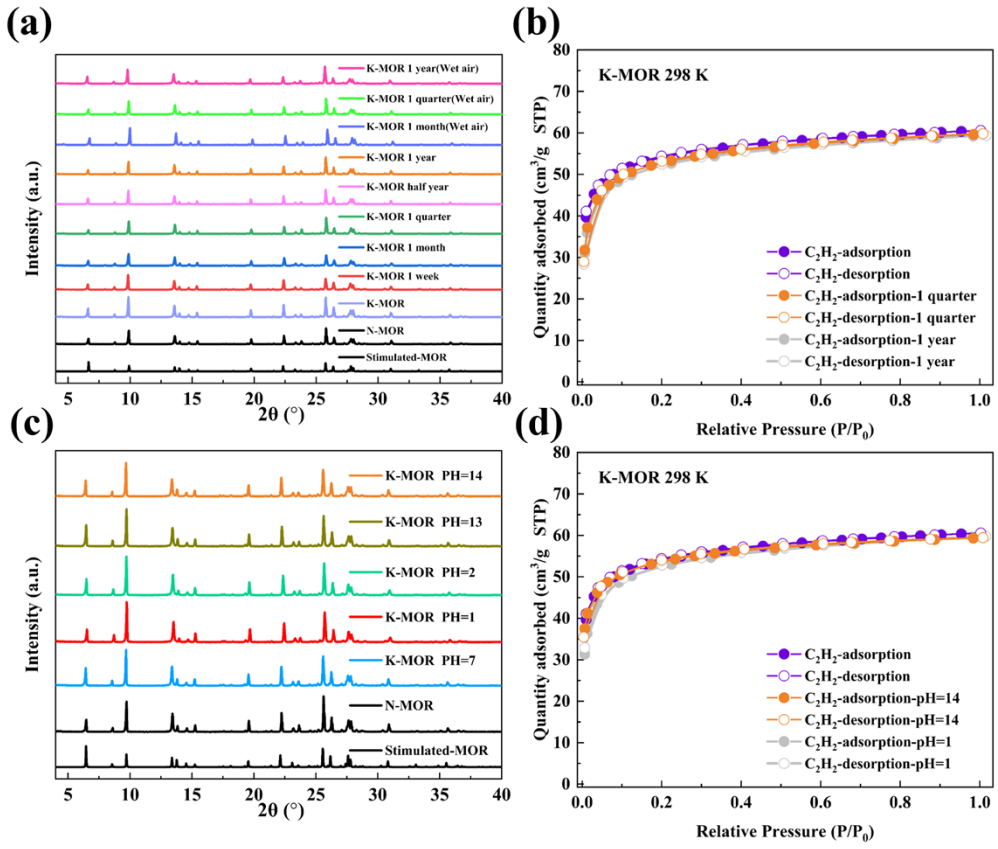

Fig. S10. (a) XRD patterns of K-MOR soaked in different wet conditions and (b) sorption isotherms of C_2H_2, (c) XRD patterns of K-MOR soaked in different pH solutions and (d) sorption isotherms of C_2H_2.

Dual-site Langmuir-Freundlich isotherm model

The uptake of C_2H_2 and C_2H_4 was described using a dual-site Langmuir isotherm model, which is formulated as:

$$q = \frac{q_c \times k_c \times P^{n_c}}{1 + k_c \times P^{n_c}} + \frac{q_i \times k_i \times P^{n_i}}{1 + k_i \times P^{n_i}}$$

The double-site Langmuir model involves parameters such as q_c($cm^3\ g^{-1}$) and q_i ($cm^3\ g^{-1}$), which represent the saturation capacities of sites *c* and *i*; as well as k_c and k_i, which are the corresponding adsorption equilibrium constants that reflect the affinity coefficients of sites *c* and *i*, respectively. The model is based on the equilibrium pressure, which is denoted as *P*.

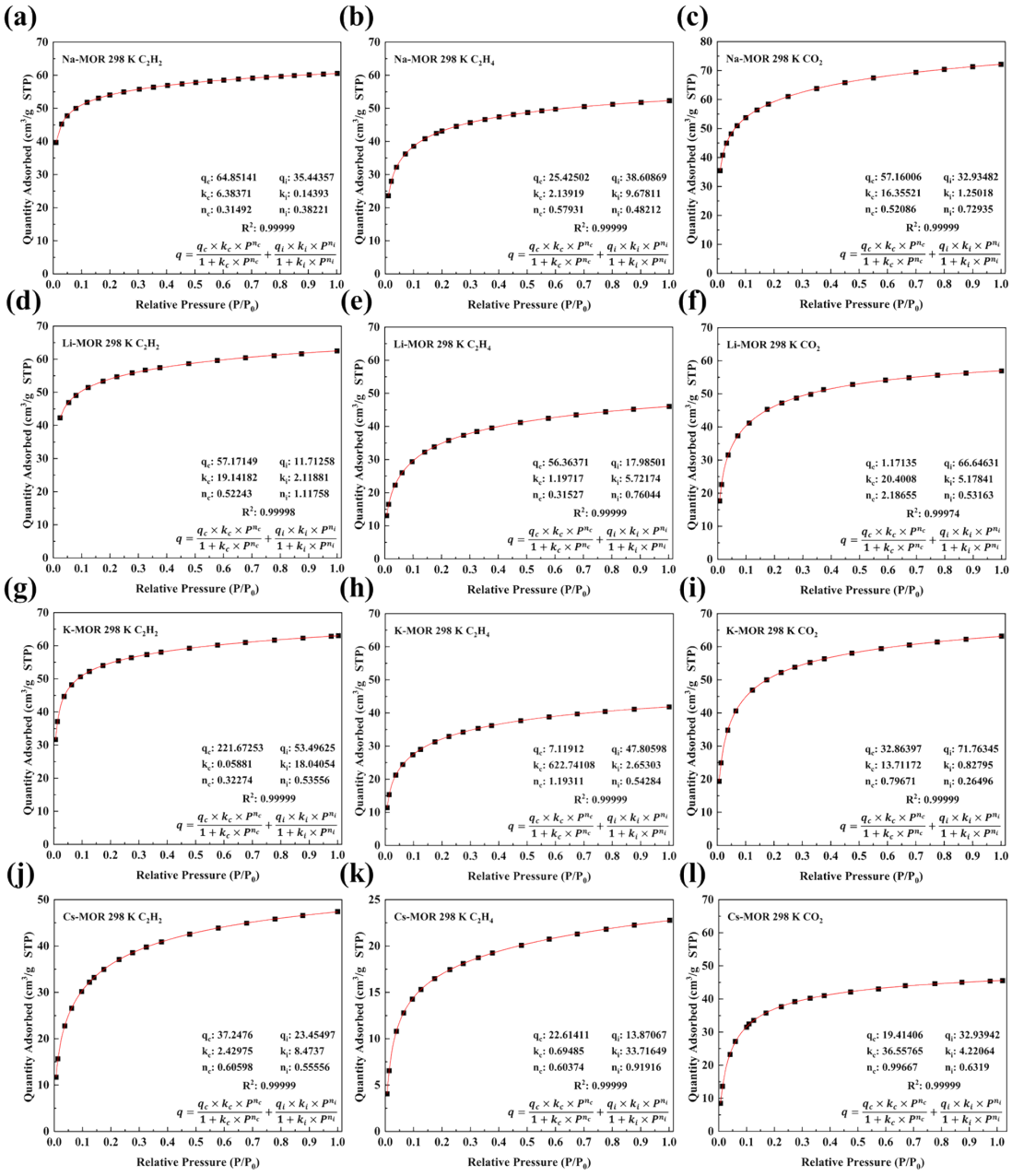

Fig. S11. Non-linear fitted curves for the C_2H_2, C_2H_4, and CO_2 sorption of (a-c) N-MOR, (d-f) Li-MOR, (g-i) K-MOR, and (j-l) Cs-MOR.

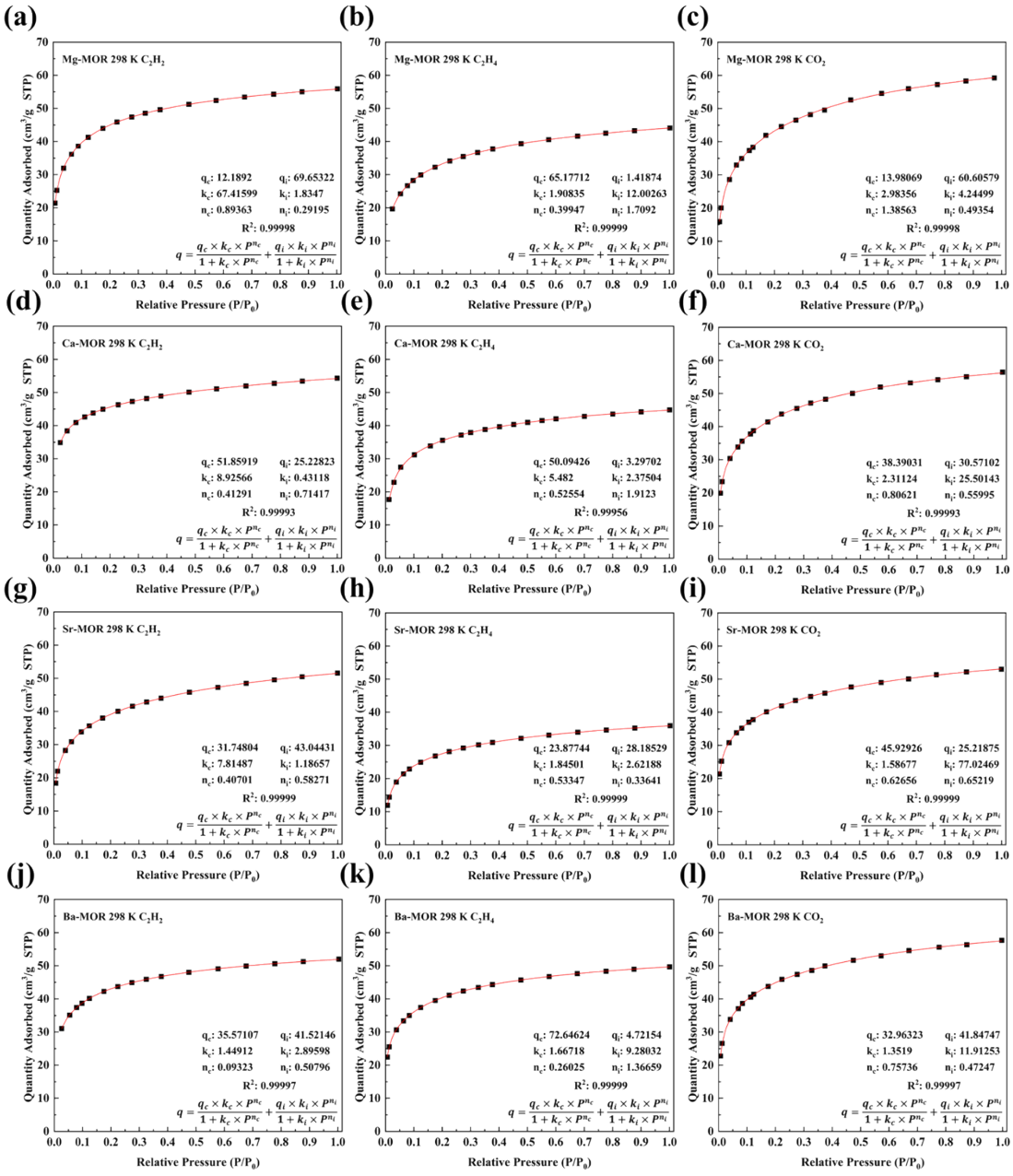

Fig. S12. Non-linear fitted curves for the C_2H_2, C_2H_4, and CO_2 sorption of (a-c) Mg-MOR, (d-f) Ca-MOR, (g-i) Sr-MOR, and (j-l) Ba-MOR.

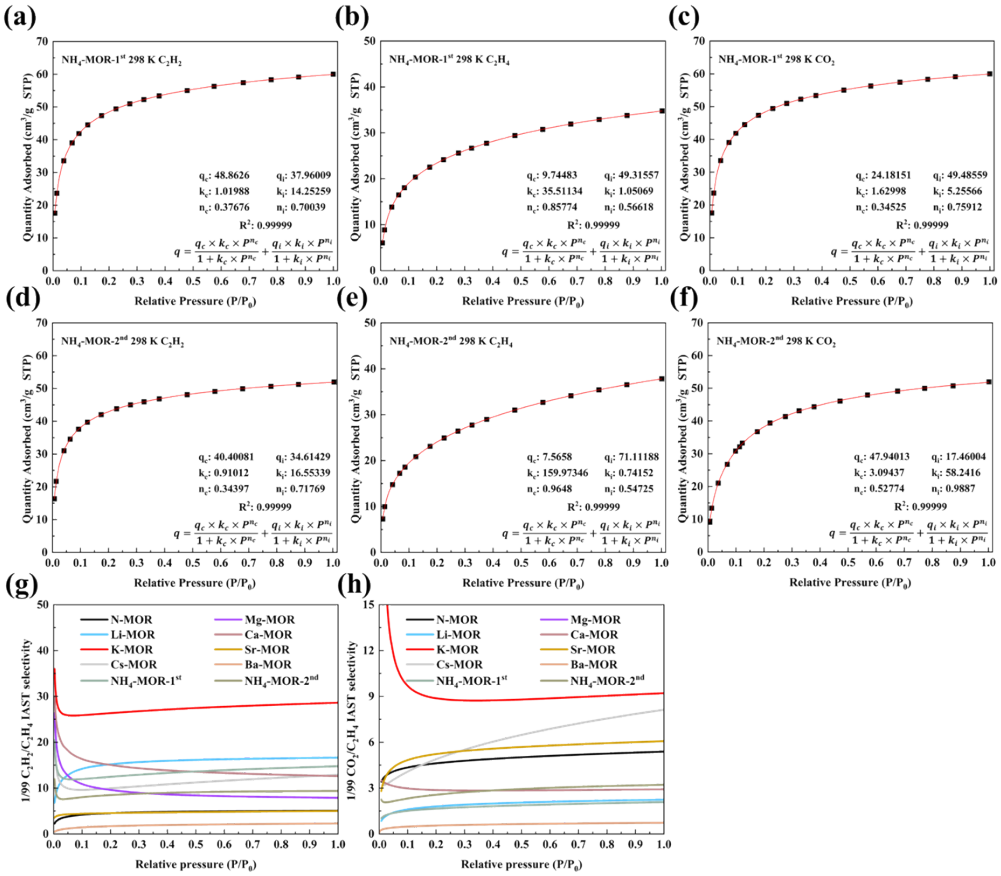

Fig. S13. Non-linear fitted curves for the C_2H_2, C_2H_4, and CO_2 sorption of (a-c) NH_4-MOR-1st, (d-f) NH_4-MOR-2nd. IAST selectivity for M-MOR on (g) 1/99 C_2H_2/C_2H_4 and (h) 1/99 CO_2/C_2H_4 mixture.

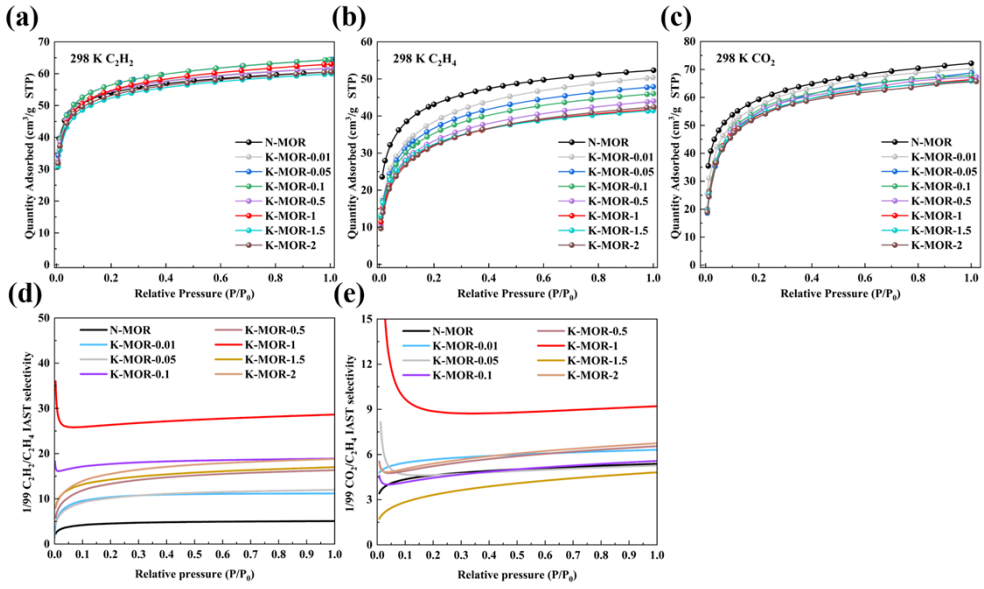

Fig. S14. (a) C_2H_2, (b) C_2H_4, and (c) CO_2 adsorption isotherms of K-MOR-X (X = 0.01, 0.05, 0.1, 0.5, 1.5, and 2) and N-MOR. IAST selectivity for K-MOR-X on (d) 1/99 C_2H_2/C_2H_4 and (e) 1/99 CO_2/C_2H_4 mixture.

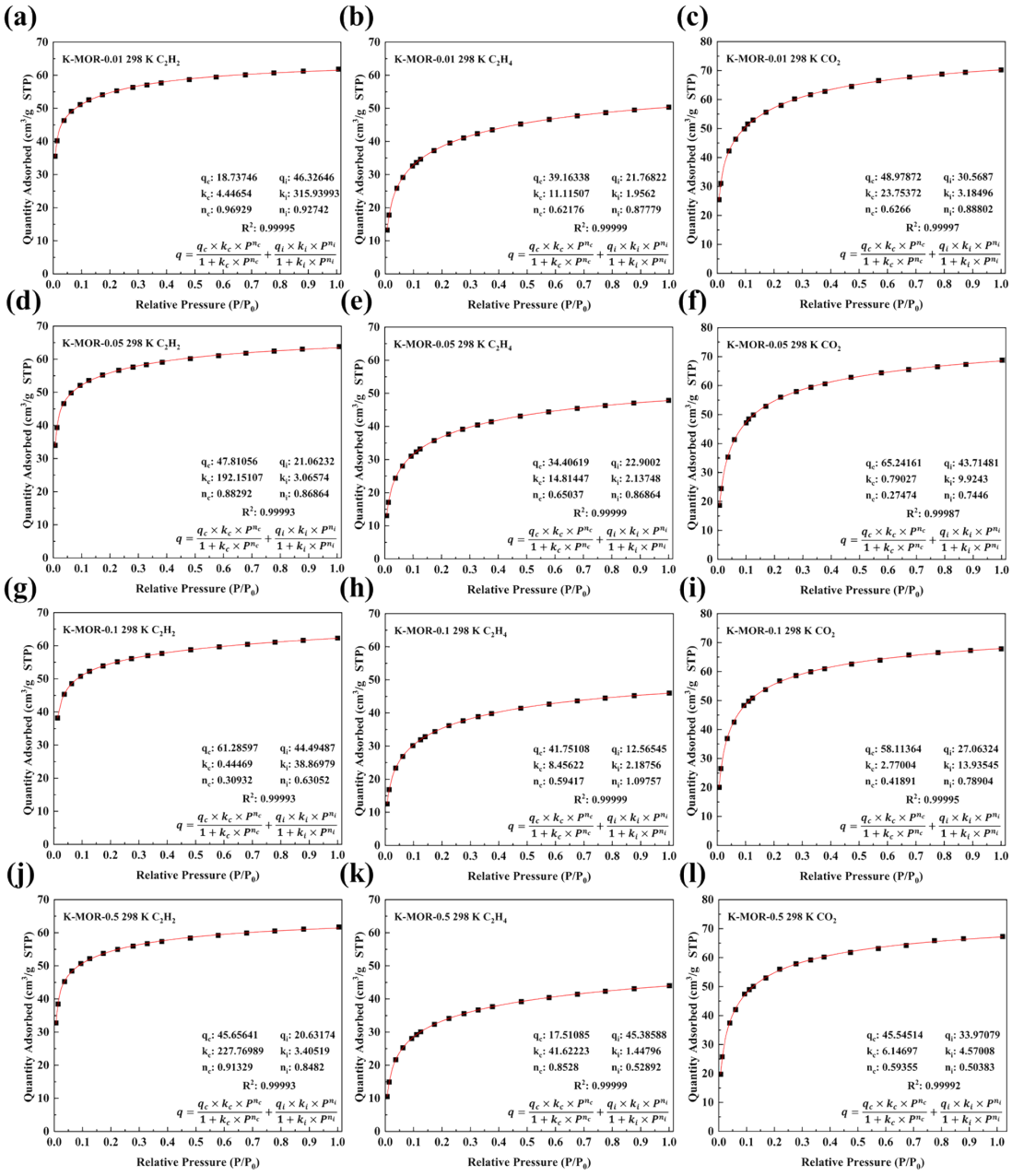

Fig. S15. Non-linear fitted curves for the C_2H_2, C_2H_4, and CO_2 sorption of (a-c) K-MOR-0.01, (d-f) K-MOR-0.05, (g-i) K-MOR-0.1, and (j-l) K-MOR-0.5.

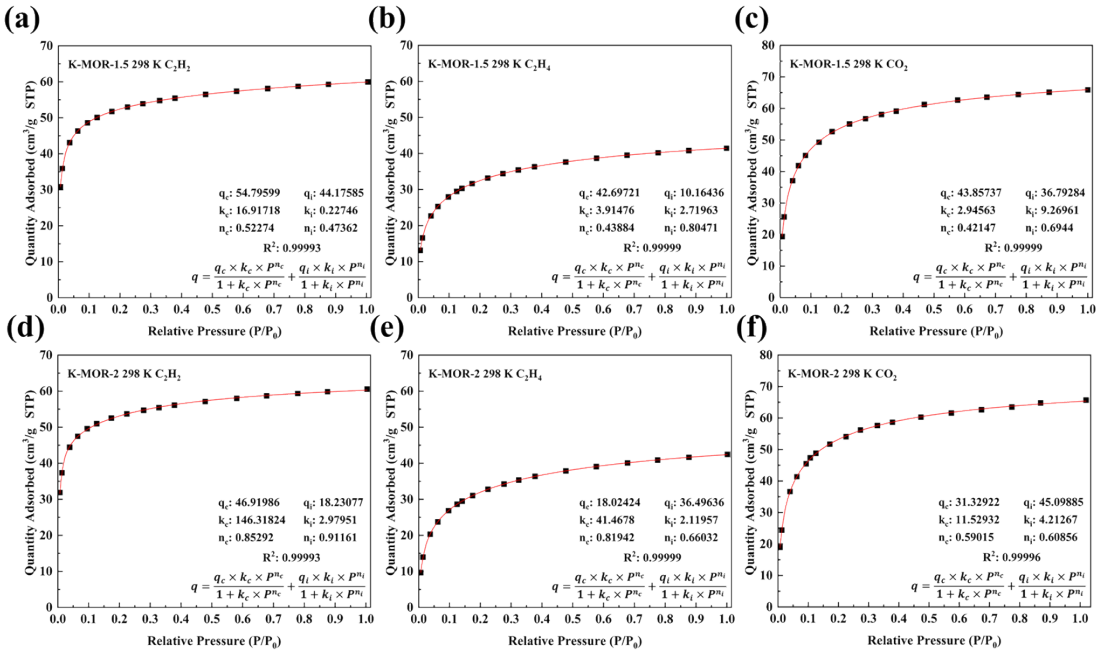

Fig. S16. Non-linear fitted curves for C_2H_2, C_2H_4, and CO_2 sorption of (a-c) K-MOR-1.5 and (d-f) K-MOR-2.

Isosteric heat adsorption (Q_{st})

Isotherms for C_2H_2, C_2H_4, and CO_2 sorption were measured at 298 K, 318 K, and 338 K, these isotherms were initially fitted to the virial equation:

$$\ln P = \ln N + \frac{1}{T}\sum_{i=0}^{m} a_i N^i + \sum_{i=0}^{n} b_i N^i$$

Where N is the amount of gas adsorbed at the pressure P, a and b are virial coefficients, m and n are the number of coefficients require to adequately describe the isotherm.

To calculate the Q_{st} values, the fitting parameters obtained from equation were then plugged into the following equation:

$$Q_{st} = -R\sum_{i=0}^{m} a_i N^i$$

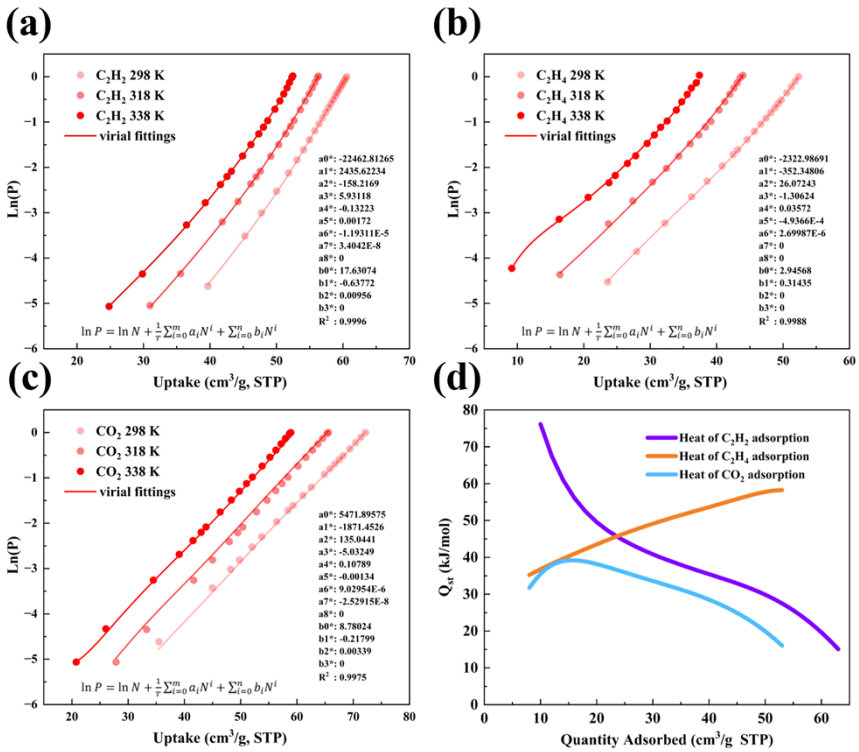

Fig. S17. Virial fitting of (a) C_2H_2, (b) C_2H_4, and (c) CO_2 adsorption of N-MOR, (d) Isosteric heats of adsorption of C_2H_2, C_2H_4, and CO_2 of N-MOR.

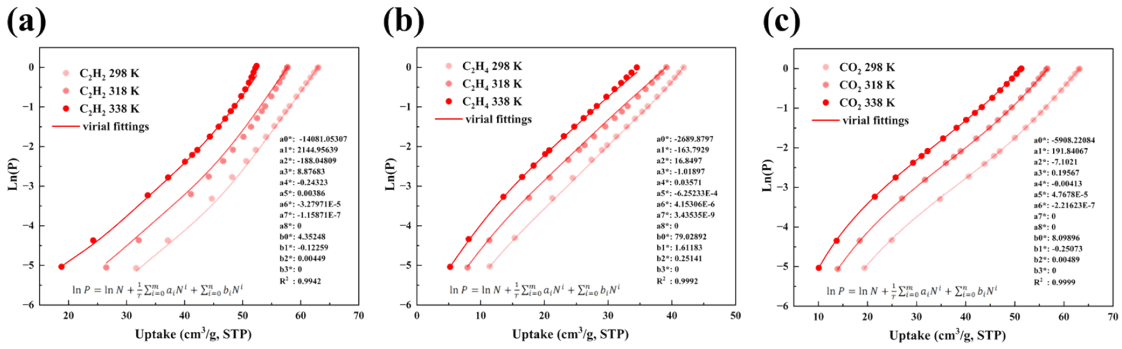

Fig. S18. (a-c) Virial fitting of (a) C_2H_2, (b) C_2H_4, and (c) CO_2 adsorption of K-MOR.

Breakthrough Experiments

All mixture gases were provided by Jining XieLi Special Gas Co., Ltd, the outlet gas was detected by Agilent GC490 gas chromatography.

Table S3. Detection of gases

Gas	Detection sensitivity	Carrier gas	Detection of the channel
He	10 ppm	Argon	Channel-1
CO_2	10 ppm	Helium	Channel-2
C_2H_4	10 ppm	Helium	Channel-2
C_2H_6	10 ppm	Helium	Channel-2
C_2H_2	10 ppm	Helium	Channel-2

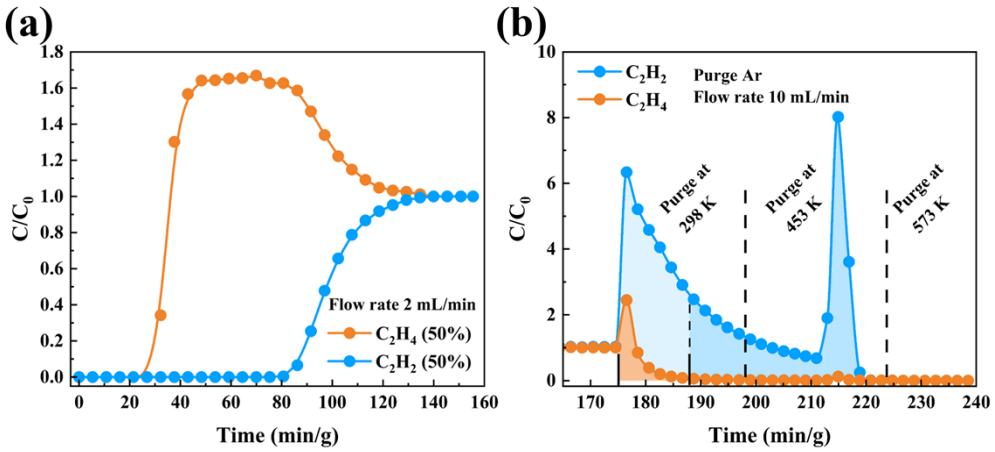

Fig. S19. C_2H_2/C_2H_4 (50/50, v/v) breakthrough experiment: (a) Breakthrough curves, (b) Desorption curves.

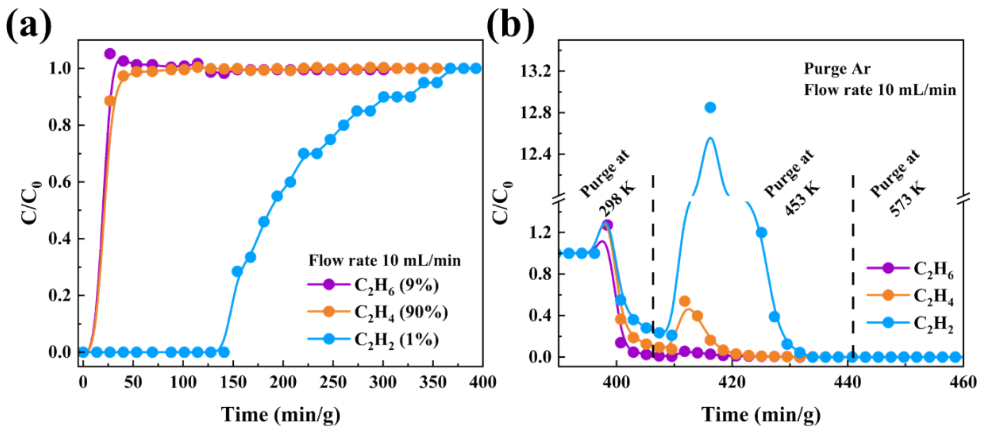

Fig. S20. $C_2H_2/C_2H_4/C_2H_6$ (1/90/9, v/v/v) breakthrough experiment: (a) Breakthrough curves, (b) Desorption curves.

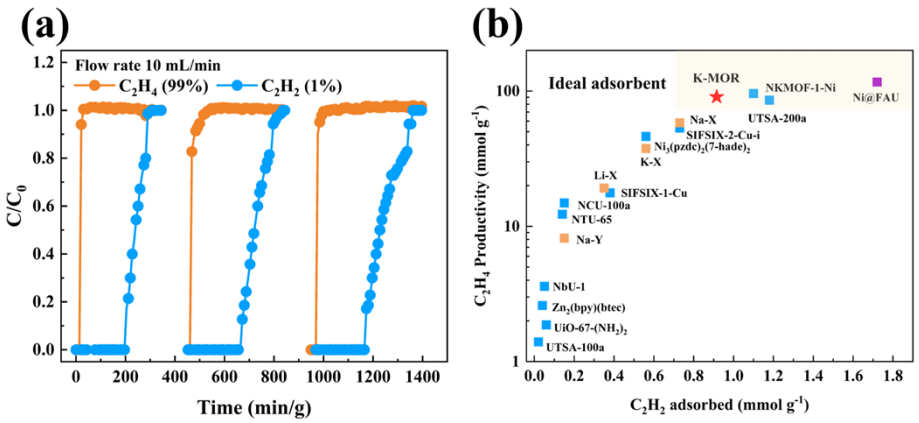

Fig. S21. (a) C_2H_2/C_2H_4 (1/99, v/v) cycling breakthrough tests on K-MOR and (b) Comparing with other materials for C_2H_4 productivity.

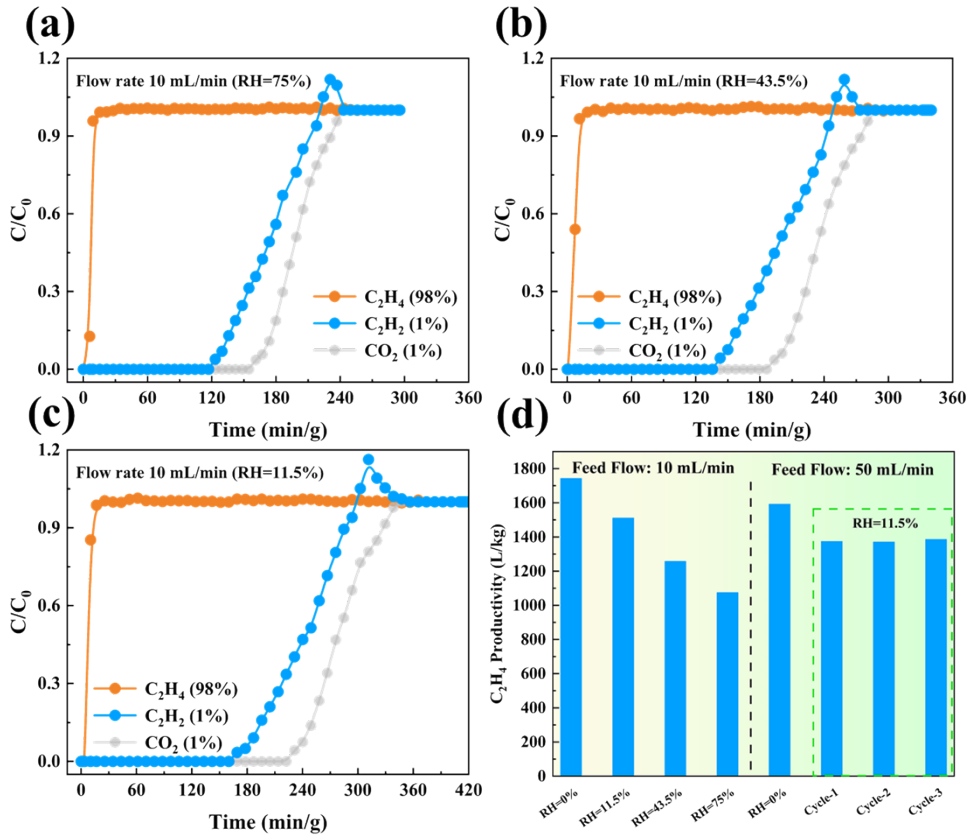

Fig. S22. (a-c) $CO_2/C_2H_2/C_2H_4$ (1/1/98, v/v/v) breakthrough experiment under different humidity levels and (d) C_2H_4 productivity calculated from these breakthrough experiments.

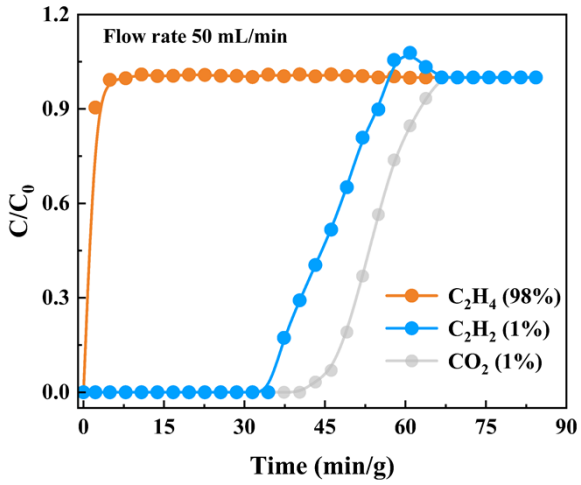

Fig. S23. $CO_2/C_2H_2/C_2H_4$ (1/1/98, v/v/v) breakthrough experiment with higher flow rate: 50 mL/min.

Table S4. Performance of solid adsorbents in C_2H_2/C_2H_4 (1/99) separation under ambient conditions[1-13].

Adsorbent	Gas flow rate (mL min^{-1})	C_2H_2 adsorbed (mmol g^{-1})	C_2H_4 Productivity (mmol g^{-1})	Dynamic Selectivity
Na-Y	10	0.15	8.18	7
Li-X	10	0.35	19.2	21
Na-X	10	0.73	58.3	44
K-X	10	0.56	37.6	34
SIFSIX-1-Cu	1.25	0.38	17.7	11
SIFSIX-2-Cu-i	1.25	0.73	53.3	45
NKMOF-1-Ni	10	1.1	96	44
UTSA-100a	2	0.02	1.4	35
UTSA-200a	2	1.18	85.7	/
UTSA-300a	2	0.04	0.7	8
Ni@FAU	6	1.72	116.8	97
NbU-1	1	0.05	3.6	10
ZJU-74a	2	0.13	12.2	5
NTU-65	3	0.14	12.3	8
NCU-100a	2	0.15	14.9	30
TJT-100	2	0.02	1.8	8.5
$Ni_3(pzdc)_2(7Hade)_2$	1.5	0.56	46.2	25
$Zn_2(bpy)(btec)$	1.25	0.04	2.6	19
UiO-67-$(NH_2)_2$	1.25	0.06	1.87	1.55
K-MOR	**10**	**0.915**	**90.6**	**54**

Details of Stimulation

The GCMC simulations were conducted to determine the ideal location of Na^+ and K^+ in the **MOR** structure. The **MOR** framework and cations were treated as rigid bodies, and the fixed loading task and Metropolis method were employed to simulate optimal adsorption sites at 298 K and 1.0 bar. The loading steps, equilibration steps, and production steps were all set to 1.0×10^7. Additionally, optimal adsorption densities for C_2H_2, C_2H_4, and CO_2 in **MOR** were simulated under the same conditions using the fixed loading task and Metropolis method, loading steps, equilibration steps, and production steps were all set to 1.0×10^7.

The interactions between the skeleton and gases, as well as between gas molecules, were characterized using the standard COMPASS II force field. Atomic partial charges for both the **MOR** framework and gases were used in the simulation, and guest gas molecules were optimized using the DMol3 module.

Table S5. Energy of the Different T-Sites of Mordenite[14, 15].

T-site	Relative energy (K)
T1	3081
T2	3072
T3	0
T4	1678

The reported energy represents the minimum energy state of a structure containing one Al atom (and one Na cation) per unit cell. The structure is considered rigid, and the minimum energy state corresponds to the most favorable location for the extraframework cation[14].

In addition to experimental studies, computer simulation[15-17] studies were also employed to support the determination of the aluminum distribution in the zeolite framework. These simulations suggested that Al atoms are primarily located in the T3 site, and the simulation results for both experiments and simulations indicate that the order of site occupancy obtained by all methods is as follows: T3 > T4 > T1 > T2.

To ensure a fair comparison, a super unit cell (222) containing 40 Al atoms based on the experimental Si/Al ratio was built, and 40 cations were used as the equilibrium cations. Sorption simulations were then carried out for the same fixed loading of C_2H_2 (23/U.C, U.C: Unit Cell), C_2H_4 (23/U.C), and CO_2 (23/U.C) in N-MOR (blank control), and under the loading calculated from C_2H_2/C_2H_4 (50/50, v/v) breakthrough experiment (K^+: 40/U.C, C_2H_2: 64/U.C, C_2H_4: 6/U.C), C_2H_2/C_2H_4 (1/99, v/v) breakthrough experiments (K^+: 40/U.C, C_2H_2: 22/U.C, C_2H_4: 40/U.C), and $CO_2/C_2H_2/C_2H_4$ (1/1/98, v/v/v) breakthrough experiments (K^+: 40/U.C, C_2H_2: 28/U.C, C_2H_4: 4/U.C, CO_2: 35/U.C).

Table S6. Aluminum distribution of MOR zeolite with Si/Al ratio equal to 8.6.

T-site	Amount	Al occupancy
T1	16	0.078125
T2	16	0.0375
T3	8	0.26875
T4	8	0.125

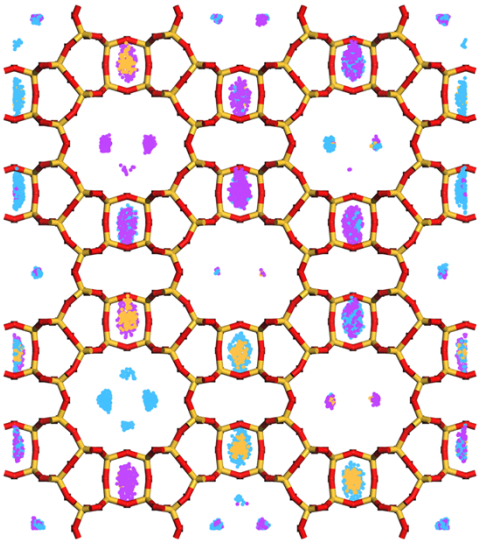

Fig. S24. Density distribution of C_2H_2 (purple), C_2H_4 (orange), CO_2 (blue), and Na^+ (omitted display) cations in N-MOR under the same fixed loading (Na^+: 40/U.C, C_2H_2: 23/U.C, C_2H_4: 23/U.C, CO_2: 23/U.C).

Reference

1 Y. Chai, X. Han, W. Li, S. Liu, S. Yao, C. Wang, W. Shi, I. da-Silva, P. Manuel, Y. Cheng, L. D. Daemen, A. J. Ramirez-Cuesta, C. C. Tang, L. Jiang, S. Yang, N. Guan and L. Li, *Science*, 2020, **368**, 1002-1006.

2 Y. Chen, Y. Du, Y. Wang, R. Krishna, L. Li, J. Yang, J. Li and B. Mu, *AIChE J.*, 2021, **67**, e17152.

3 X. Cui, K. Chen, H. Xing, Q. Yang, R. Krishna, Z. Bao, H. Wu, W. Zhou, X. Dong, Y. Han, B. Li, Q. Ren, M. J. Zaworotko and B. Chen, *Science*, 2016, **353**, 141-144.

4 Q. Dong, X. Zhang, S. Liu, R. B. Lin, Y. Guo, Y. Ma, A. Yonezu, R. Krishna, G. Liu, J. Duan, R. Matsuda, W. Jin and B. Chen, *Angew. Chem. Int. Ed.*, 2020, **59**, 22756-22762.

5 X. W. Gu, J. X. Wang, E. Wu, H. Wu, W. Zhou, G. Qian, B. Chen and B. Li, *J. Am. Chem. Soc.*, 2022, **144**, 2614-2623.

6 H. G. Hao, Y. F. Zhao, D. M. Chen, J. M. Yu, K. Tan, S. Ma, Y. Chabal, Z. M. Zhang, J. M. Dou, Z. H. Xiao, G. Day, H. C. Zhou and T. B. Lu, *Angew. Chem. Int. Ed.*, 2018, **57**, 16067-16071.

7 B. Li, X. Cui, D. O'Nolan, H. M. Wen, M. Jiang, R. Krishna, H. Wu, R. B. Lin, Y. S. Chen, D. Yuan, H. Xing, W. Zhou, Q. Ren, G. Qian, M. J. Zaworotko and B. Chen, *Adv. Mater.*, 2017, **29**, 1704210.

8 J. Li, L. Jiang, S. Chen, A. Kirchon, B. Li, Y. Li and H. C. Zhou, *J. Am. Chem. Soc.*, 2019, **141**, 3807-3811.

9 R. B. Lin, L. Li, H. Wu, H. Arman, B. Li, R. G. Lin, W. Zhou and B. Chen, *J. Am. Chem. Soc.*, 2017, **139**, 8022-8028.

10 J. Pei, K. Shao, J. X. Wang, H. M. Wen, Y. Yang, Y. Cui, R. Krishna, B. Li and G. Qian, *Adv. Mater.*, 2020, **32**, e1908275.

11 Y. L. Peng, T. Pham, P. Li, T. Wang, Y. Chen, K. J. Chen, K. A. Forrest, B. Space, P. Cheng, M. J. Zaworotko and Z. Zhang, *Angew. Chem. Int. Ed.*, 2018, **57**, 10971-10975.

12 J. Wang, Y. Zhang, P. Zhang, J. Hu, R. B. Lin, Q. Deng, Z. Zeng, H. Xing, S. Deng and B. Chen, *J. Am. Chem. Soc.*, 2020, **142**, 9744-9751.

13 Z. Zhang, S. B. Peh, R. Krishna, C. Kang, K. Chai, Y. Wang, D. Shi and D. Zhao, *Angew. Chem. Int. Ed.*, 2021, **60**, 17198-17204.

14 J. L. Schlenker, J. J. Pluth and J. V. Smith, *Mater. Res. Bull.*, 1979, **14**, 751-758.

15 M. Jeffroy, C. Nieto-Draghi and A. Boutin, *Chem. Mater.*, 2017, **29**, 513-523.

16 A. Vjunov, J. L. Fulton, T. Huthwelker, S. Pin, D. Mei, G. K. Schenter, N. Govind, D. M. Camaioni, J. Z. Hu and J. A. Lercher, *J. Am. Chem. Soc.*, 2014, **136**, 8296-8306.

17 B. Liu, E. García-Pérez, D. Dubbeldam, B. Smit and S. Calero, *J. Phys. Chem. C*, 2007, **111**, 10419-10426.